Neurobiology of Aging 74 (2019) 171–181

Contents lists available at ScienceDirect

Neurobiology of Aging

journal homepage: www.elsevier.com/locate/neuaging

In vivo hippocampal subfield shape related to TDP-43, amyloid beta, and tau pathologies

Veronika Hanko [a], Alexandra C. Apple [a], Kathryn I. Alpert [a], Kristen N. Warren [a], Julie A. Schneider [b], Konstantinos Arfanakis [b,c], David A. Bennett [b], Lei Wang [a,d,*]

[a] Department of Psychiatry and Behavioral Sciences, Northwestern University Feinberg School of Medicine, Chicago, IL, USA
[b] Rush Alzheimer's Disease Center, Rush University Medical Center, Chicago, IL, USA
[c] Department of Biomedical Engineering, Illinois Institute of Technology, Chicago, IL, USA
[d] Department of Radiology, Northwestern University Feinberg School of Medicine, Chicago, IL, USA

ARTICLE INFO

Article history:
Received 3 July 2017
Received in revised form 14 September 2018
Accepted 10 October 2018
Available online 25 October 2018

Keywords:
Alzheimer's disease
TDP-43
Neuroimaging
Hippocampus
Biomarker

ABSTRACT

Despite advances in the development of biomarkers for Alzheimer's disease (AD), accurate ante-mortem diagnosis remains challenging because a variety of neuropathologic disease states can coexist and contribute to the AD dementia syndrome. Here, we report a neuroimaging study correlating hippocampal deformity with regional AD and transactive response DNA-binding protein of 43 kDA pathology burden. We used hippocampal shape analysis of ante-mortem T1-weighted structural magnetic resonance imaging images of 42 participants from two longitudinal cohort studies conducted by the Rush Alzheimer's Disease Center. Surfaces were generated for the whole hippocampus and zones approximating the underlying subfields using a previously developed automated image-segmentation pipeline. Multiple linear regression models were constructed to correlate the shape with pathology measures while accounting for covariates, with relationships mapped out onto hippocampal surface locations. A significant relationship existed between higher paired helical filaments–tau burden and inward hippocampal shape deformity in zones approximating CA1 and subiculum which persisted after accounting for coexisting pathologies. No significant patterns of inward surface deformity were associated with amyloid-beta or transactive response DNA-binding protein of 43 kDA after including covariates. Our findings indicate that hippocampal shape deformity measures in surface zones approximating CA1 may represent a biomarker for postmortem AD pathology.

1. Introduction

As the population of the United States continues to age, dementia remains a significant contributor to both mortality and health-care costs (Hurd et al., 2013; Tinetti et al., 2012). Although Alzheimer's disease (AD)-related pathology is the most common, clinical, pathologic studies have shown that non-Alzheimer's neurodegenerative pathologies such as vascular disease, alpha-synuclein, and transactive response DNA-binding protein of 43 kDA (TDP-43) proteinopathy are much more common than was previously realized (Kovacs et al., 2013; Schneider et al., 2007a; Toledo et al., 2013) and that mixed pathologies dominate the pathologic landscape in older persons. In recent years, TDP-43—an RNA/DNA-binding protein found to be a major component of neuronal inclusions in amyotrophic lateral sclerosis and also in a subset of frontotemporal lobar degeneration cases—has been found to be associated with tauopathies such as AD pathology (Chang et al., 2016; Wilson et al., 2011). Given that so many different underlying disease processes can contribute to the AD dementia syndrome, the success of any future therapeutic treatments for neurodegenerative disorders will largely depend on the ability to achieve an early and accurate ante-mortem diagnosis.

Unfortunately, the ability to accurately identify each of the different types of neuropathologies that contribute to AD dementia remains an unmet challenge (Karageorgiou and Miller, 2014; Rohrer and Rosen, 2013). Furthermore, it is now commonly accepted that AD and related neurodegenerative conditions have a long prodromal period, during which pathologic features develop while persons remain asymptomatic (de Flores et al., 2015). Over the last decade, significant progress has been made in the discovery of molecularly specific biomarkers for AD, including cerebrospinal fluid markers for tau and amyloid-beta, as well as imaging biomarkers using positron emission tomography (PET) scanning

* Corresponding author at: Northwestern University Feinberg School of Medicine, Department of Psychiatry and Behavioral Sciences, 710 N. Lake Shore Drive, Abbott Hall 1322, Chicago, IL 60611, USA. Tel.: +312-503-3983; Fax: +312-503-0527.
E-mail address: leiwang1@northwestern.edu (L. Wang).

0197-4580/$ – see front matter © 2018 Elsevier Inc. All rights reserved.
https://doi.org/10.1016/j.neurobiolaging.2018.10.013

(Frisoni et al., 2010; Scheltens et al., 2016). Advances in the development of radioactive ligands for amyloid-beta (Jansen et al., 2015, Ossenkoppele et al., 2015; Clark et al., 2012) and to some extent tau (Villemagne et al., 2015) bring the possibility of imaging specific disease processes in vivo. However, no reliable imaging tracers for non-AD pathologies, such as alpha-synuclein, hippocampal sclerosis (HS), or TDP-43, have been found to date.

Multiple groups have used structural magnetic resonance imaging (MRI) to classify different types of dementia based on patterns of atrophy, but few can confirm their results with pathological evidence (Chow et al., 2012; Davatzikos et al., 2008; Du et al., 2007; Kim et al., 2014; Li et al., 2016; Mak et al., 2016; Thaker et al., 2017; Vemuri et al., 2011). This is problematic because a mixture of multiple neuropathologies can coexist in the brains of older adults (Schneider et al., 2007a). Several investigators have directly correlated spatial brain atrophy patterns measured from postmortem ex vivo MRI with the underlying neuropathologic disease burden obtained from autopsy data in the same subjects (Dawe et al., 2011; Kotrotsou et al., 2015). In the study by Kotrotsou et al. (2015), the authors performed ex vivo MRI on a relatively large sample of subjects from two longitudinal cohort studies who underwent autopsy and found a significant correlation between AD pathology and regional brain volumes. Although postmortem MRI techniques can enhance autopsy studies by providing fundamental insight into the connection between imaging and immunohistochemical findings, the challenge of finding useful in vivo imaging markers of neuropathology still remains. Investigators are beginning to address this problem by using ante-mortem in vivo MRI to correlate spatial brain atrophy patterns with the underlying neuropathologic disease burden (Kantarci et al., 2012; Raman et al., 2014).

In the present study, we explored the use of high-dimensional analysis of in vivo hippocampal shape based on structural MRI as biomarkers for underlying pathological disease states. Relative to other biomarkers, structural MRI is minimally invasive and an accepted component of the diagnostic workup for dementia (Knopman et al., 2001). We chose specifically to focus on the hippocampal region, as this region is the earliest to show signs of atrophy in AD and is vulnerable to other pathological disease processes as well (de Flores et al., 2015), and shape information has been shown to be more sensitive to disease progression than volume when predicting dementia onset (Csernansky et al., 2005). Hippocampal subfield analysis has also been shown to have a higher diagnostic value in preclinical stages of disease than whole hippocampal volumetry (Mueller et al., 2010). Although our goal was to identify relationships between hippocampal shape patterns and specific neuropathology burdens, we also used our surface-based zones (Csernansky et al., 2005; Wang et al., 2003) to help interpret our patterns in relationship to underlying subfields. Our group had previously demonstrated that subjects with early stage AD-type dementia showed a distinct hippocampal shape deformity that involved the CA1 and subiculum subfields compared with nondemented controls (Csernansky et al., 2004; Wang et al., 2006, 2009). We now applied a similar method to correlate ante-mortem measures of hippocampal shape with relative amounts of AD-related and TDP-43–related disease burden in the postmortem brain. Rather than limiting our study to individuals with clinically apparent AD diagnoses, we chose instead to focus on a community-based cohort of elderly adults with a mixed clinical profile (Bennett et al., 2012a,b). The rationale for this was two-fold. First, this avoided the need to make any a priori assumptions regarding pathology. Second, we hoped to capture the effect of neuropathology on hippocampal deformities at earlier, preclinical stages of the disease. We hypothesized that each of the three abnormal protein aggregates we examined (i.e., phosphorylated tau, amyloid-beta, and TDP-43) would correlate with distinct spatial patterns of hippocampal atrophy.

2. Methods and materials

2.1. Study population

Participants from two longitudinal cohort studies at the Rush Alzheimer's Disease Center were included in this work. Specifically, subjects came from either the Religious Orders Study or the Rush Memory and Aging Project (Bennett et al., 2012a,b). Participants in the Religious Orders Study consisted of older Catholic nuns, priests, or brothers from across the United States, whereas participants in the Rush Memory and Aging Project were older lay persons from across northeastern Illinois. The sole inclusion criteria were agreeing to sign an informed consent; agreeing for annual clinical evaluation, biennial MRI, and organ donation; and agreeing to sign an Anatomical Gift Act. Both studies were approved by the institutional review board at the Rush University Medical Center. All participants underwent annual detailed clinical evaluations and signed an informed consent and an anatomical gift act for brain donation upon death. Participants underwent a detailed evaluation that included medical history, neurologic examination, and 21 cognitive performance tests, 19 of which were in common. Clinical diagnostic classification of dementia, Alzheimer's dementia, and mild cognitive impairment (MCI) were made in a multistep process by a neuropsychologist and clinician as previously described (Bennett et al., 2002, 2006). Diagnoses of dementia and Alzheimer's dementia followed the recommendations of the National Institute of Neurological and Communicative Disorders and Stroke/Alzheimer's Disease and Related Disorders Association criteria (Mckhann et al., 1984) and were consistent with the revised criteria (Mckhann et al., 2011). MCI referred to the presence of cognitive impairment in the absence of dementia and were consistent with the most recent criteria (Albert et al., 2011). The Mini–Mental State Examination was used for descriptive purposes. Seventeen tests were used to summarize five cognitive domains including episodic memory, working memory, semantic memory, processing speed, and visuospatial ability, as well as a global cognitive measure based on all 17 tests. Subjects who had undergone in vivo structural MRI before death, whose autopsy findings showed any sign of AD or TDP-43 pathology, were included in this study.

2.2. Neuropathologic evaluation

Detailed procedures for postmortem brain tissue preparation and neuropathology analyses are described in previous publications (Arvanitakis et al., 2011; Bennett et al., 2004; Dawe et al., 2011; Kotrotsou et al., 2015; Schneider et al., 2004, 2007a, 2012). Here, we provide a summary of the procedures and neuropathological measures used in this work.

At autopsy, brains of the deceased subjects were removed, divided into left and right hemispheres, and one hemisphere was immersion fixed in 4% phosphate-buffered paraformaldehyde solution. The fixed hemisphere was cut into 1-cm-thick coronal slabs for subsequent tissue dissection, pathological diagnosis, and macroscopic and microscopic pathology procedures focused on the diagnosis and measurement of indices of AD and related disorders. Each case was reviewed by a board-certified neuropathologist who was blinded to age and clinical diagnoses and assigned a modified National Institute on Aging (NIA)-Reagan score for the presence and severity of AD neuropathologic changes based on consensus recommendations for postmortem diagnosis of AD, which relied on neurofibrillary tangles and plaques (Consensus recommendations, 1997; Bennett et al., 2006; Kotrotsou et al. 2015).

Amyloid-beta immunoreactive plaques were assessed in eight brain regions: (1) hippocampus CA1 and subiculum; (2) entorhinal cortex; (3) inferior temporal cortex; (4) anterior cingulate cortex; (5) angular gyrus; (6) calcarine cortex; (7) midfrontal gyrus; and (8) superior frontal gyrus. Sections were stained with a monoclonal antibody (1:50; amyloid-beta, Clone 6 F/3D, Dako) with diaminobenzidine as the reporter, with 2.5% nickel sulfate to enhance contrast. Computer-assisted sampling and image analysis were used to quantify the average percent area occupied by amyloid-beta within each cortical region. A global composite measure of amyloid-beta burden was created by averaging the regional measures and used in our statistical analyses as the primary neuropathological variable (Bennett et al. 2004).

Tau-immunoreactive neurofibrillary tangles were assessed in the same eight regions examined for amyloid-beta. Sections were stained with an paired helical filaments–tau (PHF-tau) antibody clone AT8 (Thermo Scientific; 1:2000). Computer-assisted sampling was used to quantify the density of PHF-tau–positive neuronal neurofibrillary tangles in each region (Wilson et al., 2013). A global composite measure of PHF-tau density was created by averaging the regional measures and used in our statistical analyses as the primary neuropathological variable (Bennett et al. 2004).

TDP-43 pathology was assessed in six brain regions: (1) amygdala, (2) hippocampus CA1, (3) hippocampus dentate gyrus, (4) entorhinal cortex, (5) midfrontal cortex, and (6) middle temporal cortex. Sections were stained with monoclonal antibodies to phosphorylated TDP-43 (pS409/410; 1:100). Each region of interest was rated on a 6-point scale based on the number of inclusions in a 0.25-mm^2 area of greatest density within that region (none, sparse [1-2 inclusions], sparse to moderate [3-5 inclusions], moderate [6-12 inclusions], moderate to severe [13-19 inclusions], and severe [20 or more inclusions]). A global composite measure of TDP-43 inclusions was created by summing the regional inclusions and used in our statistical analyses as the primary neuropathological variable (Wilson et al. 2013).

HS (Schneider et al., 2009), Lewy bodies, gross infarcts, atherosclerosis, arteriolosclerosis, and cerebral amyloid angiopathy (CAA) were measured and used as covariates in our study. Greater details of the assessments of these neuropathologies can be found in the publications cited herein. Lewy bodies were assessed in the substantia nigra, entorhinal cortex, anterior cingulate cortex, midfrontal cortex, superior or middle temporal cortex, and inferior parietal cortex using a monoclonal antibody to alpha-synuclein (Zymed LB 509; 1:50) (Buchman et al., 2018; Kapasi et al., 2017). Gross and microscopic infarcts were identified as previously described (Arvanitakis et al., 2011; Schneider et al., 2004) and were scored as none, one, or more than one (Schneider et al., 2007b). Atherosclerosis was assessed based on the extent of vascular involvement at the circle of Willis, whereas arteriolosclerosis was determined by the severity of wall thickening and luminal occlusion of small arterioles in sections of the anterior basal ganglia (Arvanitakis et al., 2017; Kotrotsou et al., 2015). CAA was assessed on paraffin-embedded sections from the angular gyrus, midfrontal, temporal, and calcarine cortices, as previously described (Boyle et al., 2015; Kotrotsou et al., 2015). Atherosclerosis, arteriosclerosis, and CAA were all rated on a 4-point scale from none to severe (Arvanitakis et al., 2017).

2.3. Image acquisition, segmentation, and processing: hippocampal surface plus subfield zone generation

High-resolution T1-weighted anatomical data were obtained ante-mortem on a 1.5 Tesla GE (General Electric, Waukesha, WI) MRI scanner, using a 3D magnetization–prepared rapid acquisition gradient echo sequence with the following parameters: Echo Time = 2.8 ms, Repetition Time = 6.3 ms, Field of View = 24 cm × 24 cm, flip angle = 8°, 160 slices, slice thickness of 1 mm, 224 × 192 image matrix reconstructed to 256 × 256, and 2 repetitions (Bennett et al., 2013; Stoub et al., 2005). Hippocampal segmentations were generated using a previously developed automated image-processing pipeline, multi-atlas Freesurfer-Initiated Large Deformation Diffeomorphic Metric Mapping (LDDMM) (Christensen et al., 2015; Khan et al., 2008; Wang et al., 2009). For this analysis, a multi-atlas library consisting of 74 atlas scans with previously delineated expert manual segmentations of the hippocampus was used. In each of the 74 Freesurfer-Initiated LDDMM maps, Freesurfer (Fischl et al., 2002) was used for initial alignment of subject images to each atlas image, followed by LDDMM (Beg et al., 2005) to generate hippocampal segmentations from each atlas based on high-dimensional transformations computed between the atlas and subject. A final segmentation was generated for each subject by voxel averaging the segmentations, and a surface with corresponding vertices across all subjects was propagated from a previously developed template (Csernansky et al., 2004). Visual inspection is performed after mapping to ensure data quality.

2.4. Deformation and statistical analysis on surface

To quantify hippocampal surface shape deformity, whole hippocampal surfaces for all the subjects were first rigidly aligned into a previously established template space, from which a population average was generated (Christensen et al., 2015; Csernansky et al., 2000). Perpendicular displacements were computed between corresponding vertices from this average to each subject. These displacements were then used as a measure of surface deformity for further analysis.

Statistical analysis on surfaces was performed using SurfStat in Matlab (Chung et al., 2010; Worsley et al., 2009) with a modification for univariate and multivariate data. Multiple linear regression analysis was used to investigate the association between in vivo regional hippocampal surface deformation and postmortem neuropathologic markers of AD and TDP-43 pathology. Separate models were constructed to explore the association between surface deformity and regional amyloid-beta, phosphorylated tau, and TDP-43 burden. Age at death, sex, and time between MRI and death were included as covariates. A secondary analysis was performed to include additional terms for coexisting disease processes including the other primary pathological diagnoses (PHF-tau, amyloid-beta, TDP-43), as well as HS, Lewy bodies, gross infarcts, atherosclerosis, arteriosclerosis, and CAA.

These analyses were first performed on the entire cohort (N = 42), then repeated within the healthy controls (HC) (N = 23) and combined clinical MCI + AD (N = 19) separately. Finally, to examine robustness of the outcome, we performed the following experiments: In each experiment, we removed 4 subjects (approximately 10%) at random and computed the same surface relationships accounting for the same covariates as in the original analysis. We repeated these 10 times, with 4 different subjects removed each time.

A third multivariate analysis was performed excluding the 3 subjects with a clinical diagnosis of probable AD. Finally, a fourth analysis was performed to examine the association between deformity and pathological diagnosis of AD using the NIA-Reagan Score.

In each analysis, a linear model was constructed for each vertex on the hippocampal surface map, with displacement (deformation) as the dependent variable and using neuropathology markers (TDP-43, amyloid-beta, and PHF-tau) and covariates as independent predictors (age at death, sex, time between MRI and death, and coexisting pathology including cerebrovascular disease, Lewy bodies, and HS). To control for multiple comparisons, the Random Field

Theory (Adler and Society for Industrial and Applied Mathematics 2010; Adler and Hasofer, 1976; Worsley, 2005) was applied (within SurfStat). Because signals (i.e., hippocampal deformations) at neighboring vertices are necessarily correlated and therefore may be spatially continuous (i.e., forming clusters), multiple comparison correction methods such as Bonferroni or false discovery rate (Genovese et al., 2002) are not appropriate as they only consider the peak of significance at individual vertices (Perneger, 1998). The Random Field Theory, however, considers both peaks and spatial extent of the signal by modeling the noise as Gaussian random fields (Chumbley and Friston, 2009). This approach produced significant clusters of vertices at a desired family-wise error rate (e.g., $p < 0.05$). Significant beta-coefficients were visualized as color-maps superimposed on the population average hippocampal surface. To aid the visual interpretation of the patterns of relationships, template-based surface zones approximating the underlying CA1, subiculum, and combined CA2-4 and dentate gyrus hippocampal subfields, as previously described (Christensen et al., 2015; Csernansky et al., 2005; Wang et al., 2003), were used.

3. Results

3.1. Ante-mortem population characteristics

Demographic information including age at the time of MRI scan, age at death, sex, and number of years of education is provided in Table 1. Total average left hippocampal volume (standard deviation) was 2787 (438) mm^3 and right 2877 (487) mm^3. Overall, subjects had a spectrum of ante-mortem clinical diagnoses. Of the 42 subjects, 23 were determined to be cognitively normal (CN), 16 had a clinical diagnosis of MCI, and three had probable AD. The three subjects with AD were impaired in memory by definition. Of the 16 subjects with MCI, nine were classified as amnestic (56%).

3.2. Distribution of neuropathologies across subjects

The presence of various neuropathologic markers upon autopsy is summarized in Table 2. Amyloid-beta was fairly evenly distributed across brain regions, whereas PHF-tau was more localized to the entorhinal cortex, hippocampus, and mesial temporal cortex. For TDP-43, the area most affected in subjects was the amygdala (42.5%), followed by hippocampal CA1 (31%) and dentate gyrus (14%). Of the 42 subjects, 25 received a postmortem pathologic diagnosis of AD using modified NIA-Reagan scores (i.e., intermediate or high scale) (Bennett et al., 2006). The majority (88%) also had at least one non-AD neuropathology, including TDP-43 pathology (n = 17: 6, localized to amygdala; 10, extension to hippocampus and/or entorhinal cortex; 1, extension to the neocortex), Lewy body diseases (n = 9: 1, nigral predominant; 6, limbic type; 2, neocortical type), HS (3), and cerebral infarctions (7, gross only; 8, microchronic only; 8, both). Coexisting cerebrovascular pathologies were also common, including CAA (n = 32: 23, mild; 8, moderate; 1, severe), cerebral atherosclerosis (n = 32: 23, mild; 8, moderate; 1, severe), and arteriolosclerosis (n = 27: 17, mild; 9, moderate; 1, severe).

3.3. Relationship between neuropathologic burden and hippocampal surface deformity

Fig. 1 shows hippocampal surface maps representing the relationship between global PHF-tau, amyloid-beta, and TDP-43 levels and hippocampal surface deformity for all 42 subjects before and after accounting for coexisting pathology. Without accounting for coexisting pathology, the higher global PHF-tau burden was associated with more inward deformity in surface zones approximating the CA1 and the subiculum, higher global amyloid-beta burden was associated with inward deformity in the surface zone approximating subiculum, and higher global TDP-43 levels were associated with inward deformity in the surface zone approximating CA1. Associations with each pathology demonstrate a distinct spatial pattern. After accounting for the coexisting pathology, the relationship observed between higher PHF-tau burden and increased inward deformity in hippocampal surface zones approximating CA1 and subiculum remained. However, when covariates were included, the relationships previously observed for amyloid-beta and TDP-43 were no longer significant. In the experiments examining robustness of the outcome, nine out of the 10 experiments showed similar spatial patterns (not shown) as the original analysis.

In Fig. 2, the left column shows hippocampal surface maps representing the relationship between global PHF-tau, amyloid-beta, and TDP-43 levels and hippocampal surface deformity in the

Table 1
Demographic information of the 19 MCI + AD participants

Characteristics	Value
N	42
Male, n (%)	17 (40%)
Age at visit (mean, SD) [range, median]	87.6, 5.0 [77.1–100.2, 87.1] y
Age at death (mean, SD) [range, median]	90.4, 5.0 [79.5–102.6, 89.5] y
Time from last MRI to death (mean, SD) [range, median]	2.7, 1.2 [0.17–4.8, 2.6] y
Years of education (mean, SD) [range, median]	15.0, 3.3 [8.0–22.0, 15.0] y
Ante-mortem clinical diagnosis, n (%)	
NL	23 (54.7%)
MCI	16 (38.1%)
AD	3 (7.2%)

Of the 19 participants, 12 (63%) were classified as being impaired in the memory domain. Within the MCI group alone, 9 out of 16 were classified as amnestic (56%).
Key: AD, probable Alzheimer's disease–dementia; MCI, mild cognitive impairment; MRI, magnetic resonance imaging; NL, normal cognition; SD, standard deviation.

Table 2
Summary of neuropathologic findings at autopsy

Characteristics	N (%)
PHF-tau	
Global	42 (100)
Hippocampal	42 (100)
Amyloid-beta	
Global	38 (90.4)
Hippocampal	26 (64.3)
TDP-43	
Global	18 (42.8)
Hippocampal	13 (30.9)
Lewy bodies	8 (19.0)
Hippocampal sclerosis	3 (7.1)
Cerebral amyloid angiopathy	32 (76)
Atherosclerosis	
None	10 (23.8)
Mild	23 (54.8)
Moderate	8 (19.0)
Severe	1 (2.4)
Arteriolosclerosis	
None	15 (35.7)
Mild	17 (40.5)
Moderate	9 (21.4)
Severe	1 (2.4)
Chronic infarcts (any size)	
None	19 (45.2)
One	12 (28.6)
Multi-infarct	11 (26.2)

Global amyloid-beta and tangle scores were computed by taking a mean across 8 regions (hippocampus, entorhinal cortex, midfrontal gyrus, inferior temporal, anterior gyrus, calcarine cortex, cingulate region, and superior frontal gyrus).
Key: TDP-43, transactive response DNA-binding protein of 43 kDA.

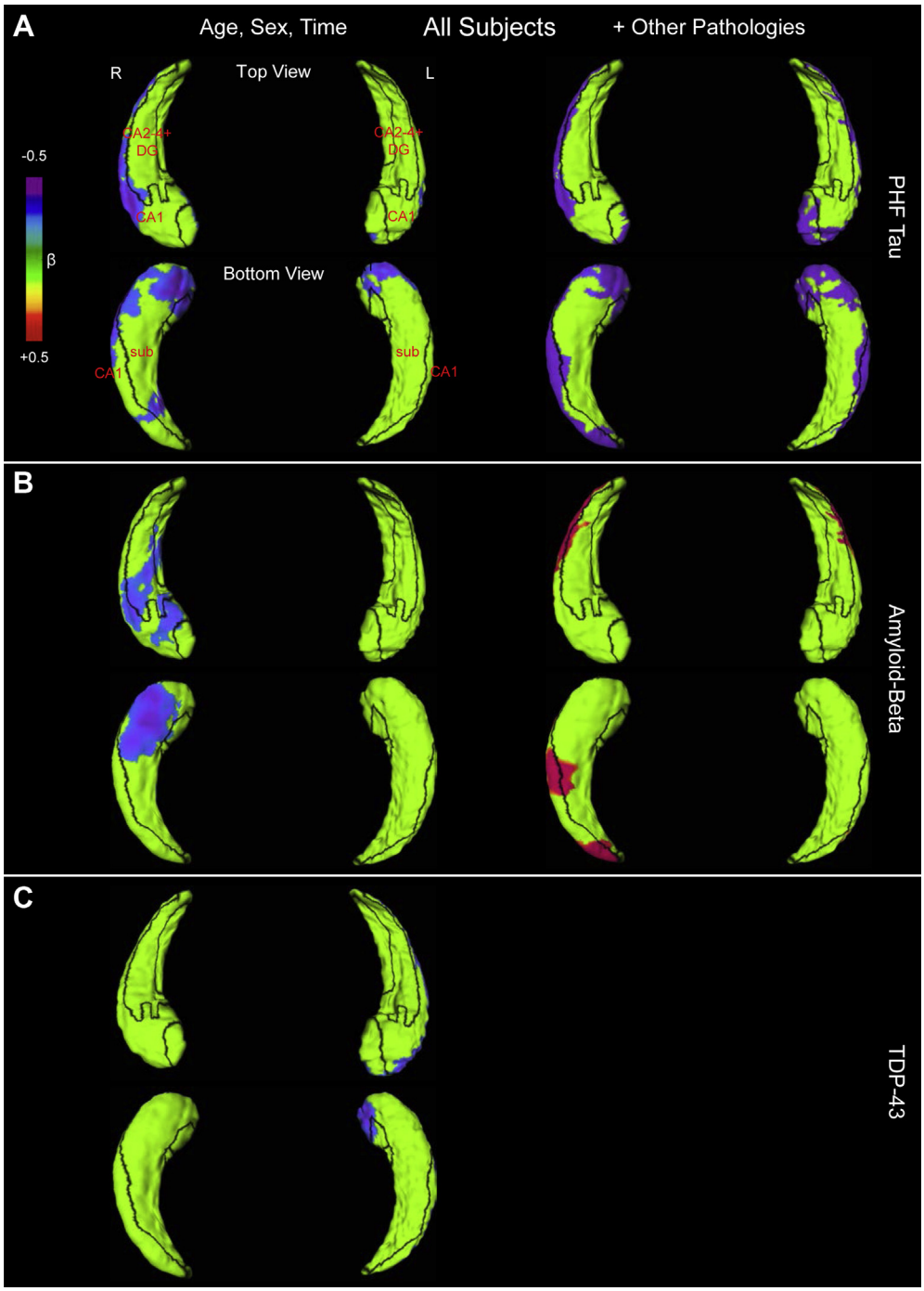

Fig. 1. Visualization of the relationship between global immunohistochemical pathology burden and hippocampal surface deformity for PHF-tau (A), amyloid-beta (B), and TDP-43 (C) for all subjects. Left panels show results of univariate analysis, whereas right panels show results after accounting for age, sex, and time between MRI and death, as well as coexisting pathology including cerebrovascular disease, Lewy bodies, and hippocampal sclerosis. Maps are thresholded to show only clusters that remained significant after correction for multiple comparisons using the random field theory (RFT) with a family-wise error rate (FWER) < 0.05. Empty panels indicate nonsignificance. Color-maps represent standardized beta-coefficients at each vertex for a linear model using deformity as the dependent variable and pathology score as the predictor. Darker colors represent inward surface deformation (localized volume loss). "Top View" represents surface viewed from above, with head of hippocampus pointing downward, whereas "Bottom View" represents surface as viewed from below, with head of hippocampus pointing upward. Abbreviations: CA, cornu ammonis; DG, dentate gyrus; L, left hippocampus; MRI, magnetic resonance imaging; PHF, paired helical filaments; R, right hippocampus; sub, subiculum; TDP-43, transactive response DNA-binding protein of 43 kDA. (For interpretation of the references to color in this figure legend, the reader is referred to the Web version of this article.)

19 MCI + AD subjects without accounting for coexisting pathology. The patterns of association are similar to those obtained in the entire cohort. Without accounting for coexisting pathology, higher global PHF-tau burden were associated with more inward deformity in surface zones approximating the CA1 and subiculum, higher global amyloid-beta burden was associated with more inward deformity in the surface zone approximating the CA1, and higher global TDP-43 levels were associated with more inward deformity in surface zones approximating the CA1 and subiculum. We note that the associations demonstrate a

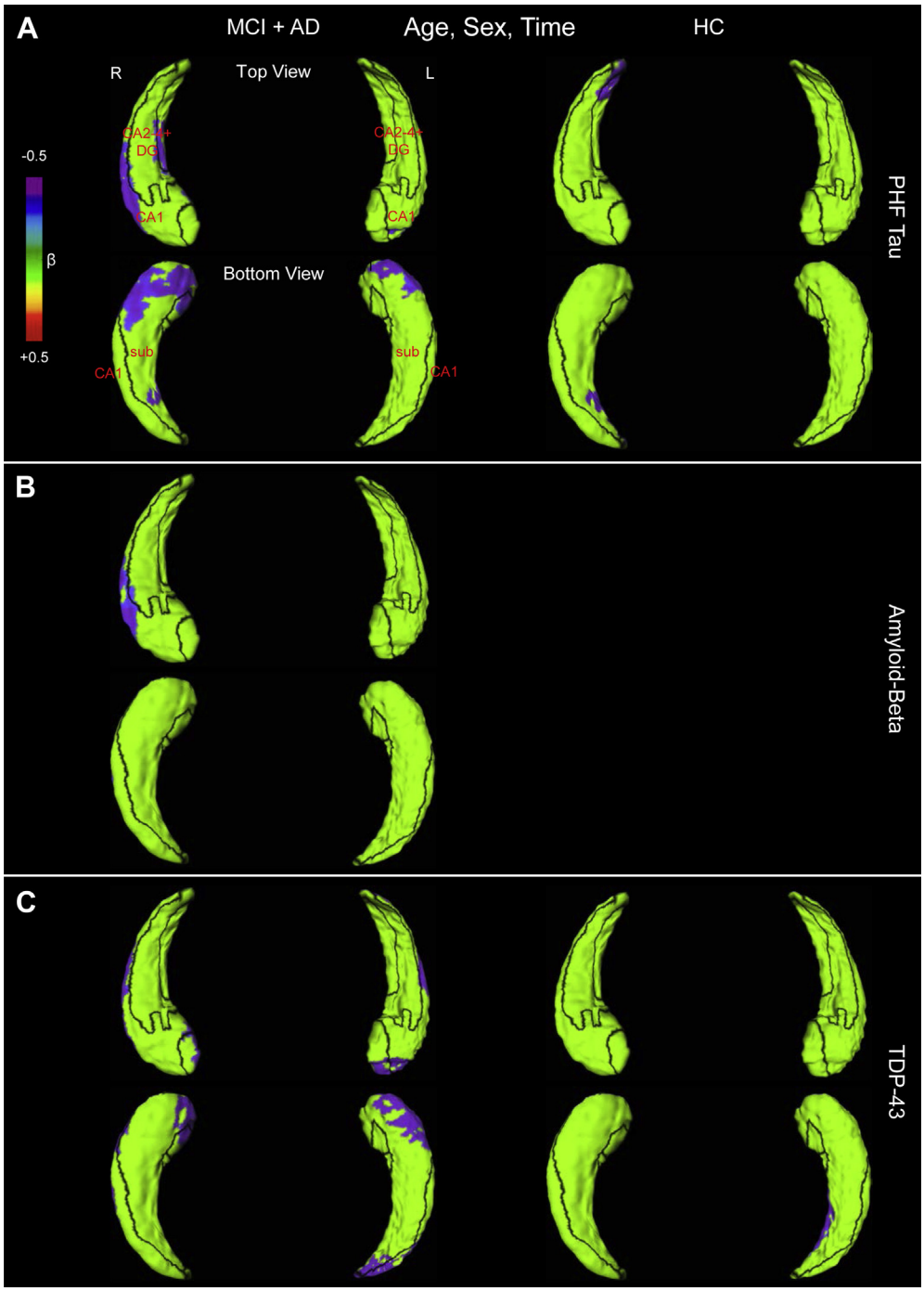

Fig. 2. Visualization of the relationship between global immunohistochemical pathology burden and hippocampal surface deformity for PHF-tau (A), amyloid-beta (B), and TDP-43 (C) for the MCI + AD (left column) and HC (right column) subjects. Panels show results of univariate analysis. Maps are thresholded to show only clusters that remained significant after correction for multiple comparisons using the random field theory (RFT) with a family-wise error rate (FWER) < 0.05. Empty panels indicate nonsignificance. Color-maps represent standardized beta-coefficients at each vertex for a linear model using deformity as the dependent variable and pathology score as the predictor. Darker colors represent inward surface deformation (localized volume loss). "Top View" represents surface viewed from above, with head of hippocampus pointing downward, whereas "Bottom View" represents surface as viewed from below, with head of hippocampus pointing upward. Abbreviations: AD, Alzheimer's disease; CA, cornu ammonis; DG, dentate gyrus; L, left hippocampus; MCI, mild cognitive impairment; PHF, paired helical filaments; R, right hippocampus; sub, subiculum; TDP-43, transactive response DNA-binding protein of 43 kDA. (For interpretation of the references to color in this figure legend, the reader is referred to the Web version of this article.)

distinct spatial pattern for each pathology. After accounting for the coexisting pathology, all relationships were no longer significant (not shown).

In Fig. 2, the right column shows hippocampal surface maps representing the relationship between global PHF-tau, amyloid-beta, and TDP-43 levels and hippocampal surface deformity in the 23 healthy control subjects before accounting for the coexisting pathology. Without accounting for the coexisting pathology, global amyloid-beta burden was not associated with hippocampal deformity, and higher PHF-tau and TDP-43 levels were associated with

more inward deformity in the surface zone approximating the subiculum. However, these associations appear to have only a minimum surface distribution. After accounting for coexisting pathology, the relationship observed between higher TDP-43 levels and more inward deformity in the surface zone approximating the subiculum remained, and the relationship previously observed for PHF-tau was no longer significant (not shown).

4. Discussion

In this study of a community-based cohort of elderly adults, we explored whether three different underlying neuropathologic processes—PHF-tau, amyloid-beta, and TDP-43—were associated with unique patterns of hippocampal deformation. When separately examined for the combined MCI + AD subjects versus HC subjects, the associations were observed largely within the MCI + AD subjects. Although several groups have previously explored the use of hippocampal shape analysis in diagnosis of various dementia subtypes (Chow et al., 2012; Christensen et al., 2015; Khan et al., 2015; Mak et al., 2016) and one has examined the relationship between postmortem hippocampal atrophy and underlying neuropathologies (Dawe et al., 2011), our study is—to our knowledge—the first to examine the association of different neuropathologies with ante-mortem hippocampal shape deformity using neuropathologically confirmed cases.

In our study, higher levels of global PHF-tau burden were associated with increased shape deformation in surface zones approximating the CA1 and the subiculum regions of the hippocampus. This is consistent with prior imaging studies that have demonstrated early involvement of the hippocampal regions approximating the CA1 subfield in AD and MCI (La Joie et al., 2013; Li et al., 2007; Scher et al., 2007; Tepest et al., 2008; Wang et al., 2003, 2006). Although all these studies relied on clinical rather than pathological classification of subjects, the fact that this relationship seems to hold when actual neuropathologic markers are taken into account yields credibility to the use of hippocampal subfield analysis as a biomarker for AD-specific neuropathology. That PHF-tau burden specifically correlated with selective atrophy in the surface zone approximating the CA1 region of the hippocampus further supports previous neuropathologic findings that show CA1 is one of the earliest regions affected by neurofibrillary tangle deposition (Braak and Braak, 1991; Schonheit et al., 2004; Fukitani et al., 2000). Furthermore, it has been shown that atrophy on MRI correlates with tau immunostaining burden (Whitwell et al., 2008). One must be cautious when making clinical inferences based solely on the presence of tau pathology and hippocampal atrophy, as these findings can also be present in a significant proportion of the “CN” elderly population (Arriagada et al., 1992b; Lace et al., 2009; Price et al., 1991). Nevertheless, in one recent structural MRI study, investigators noted a relationship between subjective cognitive decline—a self-reported perception of memory problems that is not picked up on during routine neuropsychologic testing—and selective atrophy of the hippocampal CA1 region (Perrotin et al., 2015). If hippocampal atrophy can indeed be identified on structural MRI in preclinical stages of disease years before the development of MCI, further exploration of this biomarker as a clinical screening tool may be warranted.

With regard to amyloid-beta, the relationship between neuropathologic disease burden and hippocampal subfield deformity was less clear. Although increased inward deformity of the surface zone approximating the subiculum was related to increased amounts of global amyloid-beta burden, this relationship did not hold when covariates were accounted for. A recent study by Hsu et al. combining the use of structural MRI and amyloid-PET scanning found that the amyloid-beta positive group had a significantly smaller hippocampal tail, presubiculum, subiculum, and total hippocampal gray matter volume than the amyloid-beta negative group, whereas the groups did not differ in size of CA1, CA2/3, or CA4/dentate gyrus (Hsu et al., 2015). Although several other amyloid-PET imaging studies have shown relationships between amyloid-beta burden and various imaging markers of neurodegeneration (Becker et al., 2011; Chetelat et al., 2012; Dickerson et al., 2009; Storandt et al., 2009), none of these models included terms to account for the coexisting pathology. Therefore, although studies that do not account for coexisting pathologies show that amyloid-beta influences neurodegeneration in the temporal region, our results suggest that it does so by mediating other neuropathologic pathways. This could explain studies that show amyloid-beta burden itself does not correlate well with brain atrophy (Josephs et al., 2008) and falls in line with neuropathologic studies that have shown that tau pathology has a stronger temporal and spatial correlation with neuronal loss than plaques (Arriagada et al., 1992a; Musiek and Holtzman, 2015; Gomez-Isla et al., 1997) and that tau actually mediates the association of amyloid-beta with cognition (Bennett et al., 2005, 2004; Yu et al., 2014). Several investigators have hypothesized that amyloid-beta may trigger a worsening of tau-related neurodegeneration (Musiek et al., 2015; Wang et al., 2016), whereas animal studies suggest that tau mediates the toxicity of amyloid-beta (Ittner et al., 2010). Further molecular studies would be needed to test these hypotheses.

For TDP-43, we observed a relationship between TDP-43 deposition and increased inward shape deformity in the surface zone approximating CA1, with a spatial distribution that was different from that of PHF-tau. However, this pattern did not hold when we accounted for coexisting pathologies. Further studies would be needed to confirm our preliminary evidence between TDP-43 deposition and unique patterns of neurodegeneration. Nevertheless, some studies have found an association between the presence of TDP-43 and hippocampal atrophy in subjects with coexisting AD pathology (Josephs et al., 2014a,b; Josephs et al., 2015). This falls in line with neuropathologic studies that have indicated that the medial temporal lobe structures (including the hippocampus) are susceptible to TDP-43 inclusions in AD (James et al., 2016; Josephs et al., 2016; Josephs et al., 2014a,b; Hu et al., 2008). Although their exact staging schemes differ, those studies strongly suggest that TDP-43 deposition in AD begins in the amygdala, spreads to the entorhinal cortex/hippocampus, and eventually includes other areas of the cortex (James et al., 2016; Josephs et al., 2016). Future structural MRI studies should include the amygdala to capture the additional variation in patterns of AD- and TDP-related effects on neurodegeneration.

As mentioned previously, hippocampal shape deformation showed unique patterns of association with PHF-tau, amyloid-beta, and TDP-43 within the MCI + AD subjects when not accounting for coexisting pathology. These patterns were similar to those obtained in the entire cohort, especially for PHF-tau. When visually compared with the HC, the spatial distribution patterns were distinct and extended across much larger portions of the surfaces. These results suggest that the unique spatial patterns between hippocampal shape and AD and related pathologies can be potential biomarkers that could distinguish the underlying disease pathologies in patients with a clinical diagnosis. Larger number of cases should be included in the future to confirm and validate these preliminary findings. Future studies can then develop approaches in which this type of information is used to select appropriate patients for clinical trials of specific disease-altering interventions. The findings on the HC are intriguing, suggesting a preclinical disease process. Although studies have shown that some CN individuals carry AD and related pathologies, larger studies are needed to further validate our findings.

In a previously published study (Zarow et al., 2011), we used similar methods to compare hippocampal surface shape deformation between individuals with HS and AD. In that article, we argued that a clinical diagnosis of HS is rarely, if ever, made, and in fact, all HS cases from that study received a clinical diagnosis other than HS. In the present study, the amyloid-beta, PHF-tau, and TDP-43 pathologies were found in the three subjects with HS. Also, our analysis covariated for HS ratings, which were present (severe) or absent (possible or nonexistent). Therefore, our results demonstrate that ante-mortem MRI measures can relate to postmortem AD and related disorders (age-related TDP-43 pathology) pathologies despite the presence of HS, which is well aligned with our overall hypothesis. Nonetheless, more data with HS will be needed to determine whether HS with or without coexisting AD and TDP-43 pathologies also has specific shape changes.

Overall, our study had several important strengths. First, we relied on neuropathologically confirmed cases, avoiding the need for making a priori assumptions regarding neuropathologic classification. This is essential because studies have shown that presently correlations between clinical symptoms and neuropathology subtypes could be poor (Mesulam et al., 2014). Second, the fact that the subjects were drawn from two community cohorts of older individuals who were enrolled as healthy participants (some of whom later converted to MCI/AD, whereas others did not) may make the results more applicable to the general elderly population than would be had subjects been drawn from memory clinics alone. Third, our method used structural MRI, which may be a more economical alternative to other imaging techniques such as amyloid- or tau-PET, as Medicare does not routinely reimburse these novel diagnostic studies in the workup for MCI (Jacques et al., 2013). Finally, this work raises the possibility of prediction of multiple underlying neuropathologies using a single imaging study, which could be an advantage over PET methods which rely on multiple radioactive ligands.

However, our study also had some important limitations. First, the sample size was relatively small (N = 42), limiting our ability to detect subtle differences with enough power. For this reason, it would be essential to replicate these findings in larger study populations. Second, our ability to directly correlate neuroimaging with postmortem neuropathologic data was limited by the fact that pathology was examined in sparse and relatively small areas of the brain, each covering 6-20 microns, whereas whole-brain/structure coverage would have been necessary to establish a true ante-mortem/postmortem connection. Third, our study did not include results of clinical testing in the analysis. Consequently, it is difficult to draw conclusions regarding the clinical significance of hippocampal volume loss in respect to cognition. In addition, the hippocampal surface shape represented in this article does not necessarily reflect atrophy specific to certain underlying subfields. For example, atrophy of the dentate gyrus may contribute to the surface shape deformation in the CA and subiculum areas as much of the dentate gyrus is not appreciated at the surface of the hippocampus. Finally, our study population had a mean age of about 88 years at the time of imaging, which is much older than the typical age of patients presenting to memory clinics. Therefore, the relationships we observed may be different in those populations. Further studies should be carried out to validate our findings in larger study populations and to further characterize the relationship between TDP-43 burden and hippocampal shape.

Because our interpretation of the relationship between hippocampal shape and neuropathology burden was related to underlying subfields, variations on the anatomical definition of the subfields may influence the interpretation. As summarized in the study by Yushkevich et al., 2015, although there is good overlap among the 21 active hippocampal subfield segmentation protocols, differences exist as well. For example, although some protocols delineate each of the CA1-4, others combine them in different ways. Furthermore, the boundary between the CA fields and their adjacent dentate gyrus and subiculum varies depending on the atlases used. Similar issues exist among automatic subfield methods (Mueller et al., 2018). Therefore, when localizing our observed relationships between the hippocampal shape and neuropathology burdens to underlying subfields, caution should be exercised.

There is a complex set of correspondences between dementia-related syndromes and neuropathologies, which makes accurate ante-mortem diagnosis difficult. Recent studies have shown that patients often carry a mixture of neuropathologies. For example, a significant number of clinical AD cases demonstrate admixtures of amyloid-beta and TDP-43 neuropathologies. Two decades of clinical trials of AD patients have failed to produce effective disease-modifying drugs, and an inaccurate ante-mortem diagnosis has been implicated as a key contributing factor. The present study continues the work that addresses the unmet need for ante-mortem biomarkers that can identify patients with specific neuropathologies so that future disease-altering drugs can be tested with more success. Larger numbers will be needed to further investigate the unique relationships between hippocampal deformation and specific pathologies. Amyloid and PHF-tau are measured with high precision, and there is work underway to more accurately define the quantity of TDP-43 pathology in each region. The success of disease-altering therapies depends largely on an early and specific diagnosis. Research presented in this article could lead to tools that can be used in future clinical trials to identify the most appropriate patient populations for specific disease-altering interventions. The ability to create biomarkers based on structural MRI could be a powerful tool in differentiating between AD and non-AD pathologies at preclinical stages of the disease. If and when effective disease-altering therapies are developed, our disease-predicting biomarkers can be used to select the most appropriate therapies for the patient.

Acknowledgements

The authors thank the participants of the Rush Memory and Aging Project and Religious Orders Study. The study was supported by NIH grants R01AG055121, P30AG10161, R01AG15819, R01AG17917, R01AG40039, K23AG40625, R01AG42210, and UH2NS100599.

References

Adler, R.J., Society for Industrial and Applied Mathematics, 2010. The Geometry of Random Fields. Classics in Applied Mathematics 62. SIAM Ed. Society for Industrial and Applied Mathematics (SIAM, 3600 Market Street, Floor 6, Philadelphia, PA 19104), Philadelphia, PA.

Adler, R.J., Hasofer, A.M., 1976. Level-crossings for random fields. Ann. Probab. 4, 1–12.

Albert, M.S., DeKosky, S.T., Dickson, D., Dubois, B., Feldman, H.H., Fox, N.C., Gamst, A., Holtzman, D.M., Jagust, W.J., Petersen, R.C., Snyder, P.J., Carrillo, M.C., Thies, B., Phelps, C.H., 2011. The diagnosis of mild cognitive impairment due to Alzheimer's disease: recommendations from the National Institute on Aging-Alzheimer's Association workgroups on diagnostic guidelines for Alzheimer's disease. Alzheimers Dement. 7, 270–279.

Arriagada, P.V., Marzloff, K., Hyman, B.T., 1992a. Distribution of Alzheimer-type pathologic changes in nondemented elderly individuals matches the pattern in Alzheimer's disease. Neurology 42, 1681–1688.

Arriagada, P.V., Growdon, J.H., Hedley-Whyte, E.T., Hyman, B.T., 1992b. Neurofibrillary tangles but not senile plaques parallel duration and severity of Alzheimer's disease. Neurology 42, 631–639.

Arvanitakis, Z., Leurgans, S.E., Wang, Z., Wilson, R.S., Bennett, D.A., Schneider, J.A., 2011. Cerebral amyloid angiopathy pathology and cognitive domains in older persons. Ann. Neurol. 69, 320–327.

Arvanitakis, Z., Capuano, A.W., Leurgans, S.E., Buchman, A.S., Bennett, D.A., Schneider, J.A., 2017. The relationship of cerebral vessel pathology to brain microinfarcts. Brain Pathol. 27, 77–85.

Becker, J.A., Hedden, T., Carmasin, J., Maye, J., Rentz, D.M., Putcha, D., Fischl, B., Greve, D.N., Marshall, G.A., Salloway, S., Marks, D., Buckner, R.L., Sperling, R.A., Johnson, K.A., 2011. Amyloid-beta associated cortical thinning in clinically normal elderly. Ann. Neurol. 69, 1032–1042.

Beg, M.F., Miller, M.I., Trouve, A., Younes, L., 2005. Computing large deformation metric mappings via geodesic flows of diffeomorphisms. Int. J. Comput. Vis. 61, 139.

Bennett, D.A., Wilson, R.S., Schneider, J.A., Evans, D.A., Beckett, L.A., Aggarwal, N.T., Barnes, L.L., Fox, J.H., Bach, J., 2002. Natural history of mild cognitive impairment in older persons. Neurology 59, 198–205.

Bennett, D.A., Schneider, J.A., Wilson, R.S., Bienias, J.L., Arnold, S.E., 2004. Neurofibrillary tangles mediate the association of amyloid load and with clinical Alzheimer's disease and level of cognitive function. Arch. Neurol. 61, 378–384.

Bennett, D.A., Schneider, J.A., Wilson, R.S., Bienias, J.L., Berry-Kravis, E., Arnold, S.E., 2005. Amyloid mediates the association of apolipoprotein E e4 allele to cognitive function in older people. J. Neurol. Neurosurg. Psychiatry 76, 1194–1199.

Bennett, D.A., Schneider, J.A., Arvanitakis, Z., Kelly, J.F., Aggarwal, N.T., Shah, R.C., Wilson, R.S., 2006. Neuropathology of older persons without cognitive impairment from two community-based studies. Neurology 66, 1837–1844.

Bennett, D.A., Schneider, J.A., Arvanitakis, Z., Wilson, R.S., 2012a. Overview and findings from the religious orders study. Curr. Alzheimer Res. 9, 628–645.

Bennett, D.A., Schneider, J.A., Buchman, A.S., Barnes, L.L., Boyle, P.A., Wilson, R.S., 2012b. Overview and findings from the Rush memory and aging Project. Curr. Alzheimer Res. 9, 646–663.

Bennett, D.A., Wilson, R.S., Arvanitakis, Z., Boyle, P.A., de Toledo-Morrell, L., Schneider, J.A., 2013. Selected findings from the religious orders study and Rush memory and aging Project. J. Alzheimers Dis. 33 (Supp 1), S397–S403.

Boyle, P.A., Yu, L., Nag, S., Leurgans, S., Wilson, R.S., Bennett, D.A., Schneider, J.A., 2015. Cerebral amyloid angiopathy and cognitive outcomes in community-based older persons. Neurology 85, 1930–1936.

Braak, H., Braak, E., 1991. Neuropathological staging of Alzheimer-related changes. Acta Neuropathol. 82, 239–259.

Buchman, A.S., Nag, S., Leurgans, S.E., Miller, J., VanderHorst, V., Bennett, D.A., Schneider, J.A., 2018. Spinal Lewy body pathology in older adults without an antemortem diagnosis of Parkinson's disease. Brain Pathol. 28, 560–568.

Chang, X.L., Tan, M.S., Tan, L., Yu, J.T., 2016. The role of TDP-43 in Alzheimer's Disease. Mol. Neurobiol. 53, 3349–3359.

Chetelat, G., Villemagne, V.L., Villain, N., Jones, G., Ellis, K.A., Ames, D., Martins, R.N., Masters, C.L., Rowe, C.C., AIBL Research Group, 2012. Accelerated cortical atrophy in cognitively normal elderly with high b-amyloid deposition. Neurology 78, 477–484.

Chow, N., Aarsland, D., Honarpisheh, H., Beyer, M.K., Somme, J.H., Elashoff, D., Rongve, A., Tysnes, O.B., Thompson, P.M., Apostolova, L.G., 2012. Comparing hippo-campal atrophy in Alzheimer's dementia and dementia with Lewy bodies. Dement Geriatr. Cogn. Disord. 34, 44–50.

Christensen, A., Alpert, K., Rogalski, E., Cobia, D., Rao, J., Beg, M., Weintraub, S., Mesulam, M., Wang, L., 2015. Hippocampal subfield surface deformity in non-semantic primary progressive aphasia. Alzheimers Dement. (Amst) 1, 14–23.

Chumbley, J.R., Friston, K.J., 2009. False discovery rate revisited: FDR and topological inference using Gaussian random fields. Neuroimage 44, 62–70.

Chung, M.K., Worsley, K.J., Nacewicz, B.M., Dalton, K.M., Davidson, R.F., 2010. General multivariate linear modeling of surface shape using SurfStat. Neuroimage 53, 491–505.

Clark, C.M., Pontecorvo, M.J., Beach, T.G., Bedell, B.J., Coleman, R.E., Doraiswamy, P.M., Fleisher, A.S., Reiman, E.M., Sabbagh, M.N., Sadowsky, C.H., Schneider, J.A., Arora, A., Carpenter, A.P., Flitter, M.L., Joshi, A.D., Krautkramer, M.J., Lu, M., Mintun, M.A., Skovronsky, D.M., AV-45-A16 Study Group, 2012. Cerebral PET with florbetapir compared with neuropathology at autopsy for detection of neuritic amyloid-β plaques: a prospective cohort study. Lancet Neurol. 11, 669–678.

Consensus recommendations for the postmortem diagnosis of Alzheimer's disease, 1997. The National Institute on Aging, and Reagan Institute Working Group on Diagnostic Criteria for the Neuropathological Asse. Neurobiol. Aging 18 (4 Suppl), S1–S2.

Csernansky, J.G., Wang, L., Joshi, S., Miller, A.B., Gado, M., Kido, D., McKeel, D., Morris, J.C., Miller, M.I., 2000. Early DAT is distinguished from aging by high-dimensional mapping of the hippocampus. Neurology 55, 1636–1643.

Csernansky, J.G., Wang, L., Joshi, S.C., Ratnanather, J.T., Miller, M.I., 2004. Computational anatomy and neuropsychiatric disease: probabilistic assessment of variation and statistical inference of group difference, hemispheric asymmetry, and time-dependent change. Neuroimage 23 (Suppl 1), S56–S68.

Csernansky, J.G., Wang, L., Swank, J., Miller, J.P., Gado, M., McKeel, D., Miller, M.I., Morris, J.C., 2005. Preclinical detection of Alzheimer's disease: hippocampal shape and volume predict dementia onset in the elderly. NeuroImage 25, 783–792.

Davatzikos, C., Resnick, S.M., Wu, X., Parmpi, P., Clark, C.M., 2008. Individual patient diagnosis of AD and FTD via high-dimensional pattern classification of MRI. Neuroimage 41, 1220–1227.

Dawe, R.J., Bennett, D.A., Schneider, J.A., Leurgans, S.E., Kotrotsou, A., Boyle, P.A., Arfanakis, K., 2011. Neuropathologic correlates of hippocampal atrophy in the elderly: a clinical, pathologic, postmortem MRI study. PLoS One 6, e26286.

De Flores, R., La Joie, R., Chetelat, G., 2015. Structural imaging of hippocampal subfields in healthy aging and Alzheimer's disease. Neuroscience 309, 29–50.

Dickerson, B.C., Bakkour, A., Salat, D.H., Feczko, E., Pacheco, J., Greve, D.N., Grodstein, F., Wright, C.I., Blacker, D., Rosas, H.D., Sperling, R.A., Atri, A., Growdon, J.H., Hyman, B.T., Morris, J.C., Fischl, B., Buckner, R.L., 2009. The cortical signature of Alzheimer's disease: regionally specific cortical thinning relates to symptom severity in very mild to mild AD dementia and is detectable in asymptomatic amyloid-positive individuals. Cereb. Cortex 19, 497–510.

Du, A.T., Schuff, N., Kramer, J.K., Rosen, H.J., Gorno-Tempini, M.L., Rankin, K., Miller, B.L., Weiner, M.W., 2007. Different regional patterns of cortical thinning in Alzheimer's disease and frontotemporal dementia. Brain 130, 1159–1166.

Fischl, B., Salat, D.H., Busa, E., Albert, M., Dieterich, M., Haselgrove, C., van der Kouwe, A., Kiliany, R., Kennedy, D., Klaveness, S., Montillo, A., Makris, N., Rosen, B., Dalel, A.M., 2002. Whole brain segmentation: automated labeling of neuroanatomical structures in the human brain. Neuron 33, 341–355.

Frisoni, G.B., Fox, N.C., Jack, C.R., Scheltens, P., Thompson, P.M., 2010. The clinical use of structural MRI in Alzheimer disease. Nat. Rev. Neurol. 6, 67–77.

Fukitani, Y., Cairns, N.J., Shiozawa, M., Sasaki, K., Sudo, S., Isaki, K., Lantos, P.L., 2000. Neuronal loss and neurofibrillary degeneration in the hippocampal cortex in late-onset sporadic Alzheimer's disease. Psychiatry Clin. Neurosci. 54, 523–529.

Genovese, C.R., Lazar, N.A., Nichols, T., 2002. Thresholding of statistical maps in functional neuroimaging using the false discovery rate. Neuroimage 15, 870–878.

Gómez-Isla, T., Hollister, R., West, H., Mui, S., Growdon, J.H., Petersen, R.C., Parisi, J.E., Hyman, B.T., 1997. Neuronal loss correlates with but exceeds neurofibrillary tangles in Alzheimer's disease. Ann. Neurol. 41, 17–24.

Hsu, P.J., Shou, H., Benzinger, T., Marcus, D., Durbin, T., Morris, J.C., Sheline, Y.I., 2015. Amyloid burden in cognitively normal elderly is associated with preferential hippocampal subfield volume loss. J. Alzheimers Dis. 45, 27–33.

Hu, W.T., Josephs, K.A., Knopman, D.S., Boeve, B.F., Dickson, D.W., Petersen, R.C., Parisi, J.E., 2008. Temporal lobar predominance of TDP-43 neuronal cytoplasmic inclusions in Alzheimer disease. Acta Neuropathol. 116, 215–220.

Hurd, M.D., Martorell, P., Delavande, A., Mullen, K.J., Langa, K.M., 2013. Monetary costs of dementia in the United States. N. Engl. J. Med. 368, 1326–1334.

Ittner, L.M., Ke, Y.D., Delerue, F., Bi, M., Gladbach, A., van Eersel, J., Wolfing, H., Chieng, B.C., Christie, M.J., Napier, I.A., Eckert, A., 2010. Dendritic function of tau mediates amyloid-β toxicity in Alzheimer's disease mouse models. Cell 142, 387–397.

Jacques, L., Jensen, T., Rollins, J., Coachman, B.B., Caplan, S., Hakim, R., Roche, J., Hutter, J., 2013. Decision Memo for beta amyloid Positron Emission Tomography in dementia and neurodegenerative disease (CAG-00431N). Centers for Medicare and Medicaid Services. https://www.cms.gov/medicare-coverage-database/details/nca-decision-memo.aspx?NCAId=265. (Accessed 20 December 2016).

James, B.D., Wilson, R.S., Boyle, P.A., Trojanowski, J.Q., Bennett, D.A., Schneider, J.A., 2016. TDP-43 stage, mixed pathologies, and clinical Alzheimer's-type dementia. Brain 139, 2983–2993.

Jansen, W.J., Ossenkoppele, R., Knol, D.L., Tijms, B.M., Scheltens, P., Verhey, F.R., Visser, P.J., Amyloid Biomarker Study Group, Aalten, P., Aarsland, D., Alcolea, D., Alexander, M., Almdahl, I.S., Arnold, S.E., Baldeiras, I., Barthel, H., van Berckel, B.N., Bibeau, K., Blennow, K., Brooks, D.J., van Buchem, M.A., Camus, V., Cavedo, E., Chen, K., Chetelat, G., Cohen, A.D., Drzezga, A., Engelborghs, S., Fagan, A.M., Fladby, T., Fleisher, A.S., van der Flier, W.M., Ford, L., Förster, S., Fortea, J., Foskett, N., Frederiksen, K.S., Freund-Levi, Y., Frisoni, G.B., Froelich, L., Gabryelewicz, T., Gill, K.D., Gkatzima, O., Gómez-Tortosa, E., Gordon, M.F., Grimmer, T., Hampel, H., Hausner, L., Hellwig, S., Herukka, S.K., Hildebrandt, H., Ishihara, L., Ivanoiu, A., Jagust, W.J., Johannsen, P., Kandimalla, R., Kapaki, E., Klimkowicz-Mrowiec, A., Klunk, W.E., Köhler, S., Koglin, N., Kornhuber, J., Kramberger, M.G., Van Laere, K., Landau, S.M., Lee, D.Y., de Leon, M., Lisetti, V., Lleó, A., Madsen, K., Maier, W., Marcusson, J., Mattsson, N., de Mendonça, A., Meulenbroek, O., Meyer, P.T., Mintun, M.A., Mok, V., Molinuevo, J.L., Møllergård, H.M., Morris, J.C., Mroczko, B., Van der Mussele, S., Na, D.L., Newberg, A., Nordberg, A., Nordlund, A., Novak, G.P., Paraskevas, G.P., Parnetti, L., Perera, G., Peters, O., Popp, J., Prabhakar, S., Rabinovici, G.D., Ramakers, I.H., Rami, L., Resende de Oliveira, C., Rinne, J.O., Rodrigue, K.M., Rodríguez-Rodríguez, E., Roe, C.M., Rot, U., Rowe, C.C., Rüther, E., Sabri, O., Sanchez-Juan, P., Santana, I., Sarazin, M., Schröder, J., Schütte, C., Seo, S.W., Soetewey, F., Soininen, H., Spiru, L., Struyfs, H., Teunissen, C.E., Tsolaki, M., Vandenberghe, R., Verbeek, M.M., Villemagne, V.L., Vos, S.J., van Waalwijk van Doorn, L.J., Waldemar, G., Wallin, A., Wallin, Å.K., Wiltfang, J., Wolk, D.A., Zboch, M., Zetterberg, H., 2015. Prevalence of cerebral amyloid pathology in persons without dementiaA meta-analysis. JAMA 313, 1924–1938.

Josephs, K.A., Whitwell, J.L., Ahmed, Z., Shiung, M.M., Weigand, S.D., Knopman, D.S., Boeve, B.F., Parisi, J.E., Petersen, R.C., Dickson, D.W., Jack Jr., C.R., 2008. Beta amyloid burden is not associated with rates of brain atrophy. Ann. Neurol. 63, 204–212.

Josephs, K.A., Murray, M.E., Whitwell, J.L., Parisi, J.E., Petrucelli, L., Jack, C.R., Petersen, R.C., Dickson, D.W., 2014a. Staging TDP-43 pathology in Alzheimer's disease. Acta Neuropathol. 127, 441–450.

Josephs, K.A., Whitwell, J.L., Weigand, S.D., Murray, M.E., Tosakulwong, N., Liesinger, A.M., Petrucelli, L., Senjem, M.L., Knopman, D.S., Boeve, B.F., Ivnik, R.J., Smith, G.E., Jack Jr., C.R., Parisi, J.E., Petersen, R.C., Dickson, D.W., 2014b. TDP-43 is a key player in the clinical features associated with Alzheimer's disease. Acta Neuropathol. 127, 811–824.

Josephs, K.A., Whitwell, J.L., Tosakulwong, N., Weigand, S.D., Murray, M.E., Liesinger, A.M., Petrucelli, L., Senhem, M.L., Ivnik, R.J., Parisi, J.E., Petersen, R.C., Dickson, D.W., 2015. TDP-43 and pathological subtype of Alzheimer's disease impact clinical features. Ann. Neurol. 78, 697–709.

Josephs, K.A., Murray, M.E., Whitwell, J.L., Tosukulwong, N., Weigand, S.D., Petrucelli, L., Liesinger, A.M., Petersen, R.C., Parisi, J.E., Dickson, D.W., 2016. Updated TDP-43 in Alzheimer's disease staging scheme. Acta Neuropathol. 131, 571–585.

Kantarci, K., Ferman, T.J., Boeve, B.F., Weigand, S.D., Przybelski, S., Vemuri, P., Murray, M.E., Senjem, M.L., Smith, G.E., Knopman, D.S., Petersen, R.C., Jack Jr., C.R., Parisi, J.E., Dickson, D.W., 2012. Focal atrophy on MRI and neuropathologic classification of dementia with Lewy bodies. Neurology 79, 553–560.

Kapasi, A., DeCarli, C., Schneider, J.A., 2017. Impact of multiple pathologies on the threshold for clinically overt dementia. Acta Neuropathol. 134, 171–186.

Karageorgiou, E., Miller, B.L., 2014. Frontotemporal lobar degeneration: a clinical approach. Semin. Neurol. 34, 189–201.

Khan, A., Wang, L., Beg, M.F., 2008. Freesurfer-initiated fully-automated subcortical brain segmentation in MRI using large deformation diffeomorphic metric mapping. NeuroImage 41, 735–746.

Khan, W., Westman, E., Jones, N., Wahlund, L.O., Mecocci, P., Vellas, B., Tsolaki, M., Kloszewska, I., Soininen, H., Spenger, C., Lovestone, S., Muehlboeck, J.S., Simmons, A., AddNeuroMed consortium and for the Alzheimer's Disease Neuroimaging Initiative, 2015. Automated hippocampal subfield measures as predictors of conversion from mild cognitive impairment to Alzheimer's disease in two independent cohorts. Brain Topogr 28, 746–759.

Kim, H.J., Ye, B.S., Yoon, C.W., Noh, Y., Kim, G.H., Cho, H., Jeon, S., Lee, J.M., Kim, J.H., Seong, J.K., Kim, C.H., Choe, Y.S., Lee, KH, Kin, S.T., Kim, J.S., Park, S.E., Kim, J.H., Chin, J., Cho, J., Kim, C., Lee, J.H., Weinger, M.W., Na, D.L., Seo, S.W., 2014. Cortical thickness and hippocampal shape in pure vascular mild cognitive impairment and dementia of subcortical type. Eur. J. Neurol. 21, 744–751.

Knopman, D.S., Dekosky, S.T., Cummings, J.L., Chui, H., Corey-Bloom, J., Relkin, N., Small, G.W., Miller, B., Stevens, J.C., 2001. Practice parameter: diagnosis of dementia (an evidence-based review). Rep. Qual. Stand. Subcommittee Am. Acad. Neurol. Neurol. 56, 1143–1153.

Kotrotsou, A., Schneider, J.A., Bennett, D.A., Leurgans, S.E., Dawe, R.J., Boyle, P.A., Golak, T., Arfanakis, K., 2015. Neuropathologic correlates of regional brain volumes in a community cohort of older adults. Neurobiol. Aging 36, 2798–2805.

Kovacs, G.G., Milenkovic, I., Wohrer, A., Hoftberger, R., Gelpi, E., Haberler, C., Honigschnabl, S., Reiner-Concin, A., Heinzl, H., Jungwirth, S., Krampla, W., Fischer, P., Budka, H., 2013. Non-Alzheimer neurodenerative pathologies and their combinations are more frequent than commonly believed in the elderly brain: a community-based autopsy series. Acta Neuropathol. 126, 365–384.

La Joie, R., Perrotin, A., de La Sayette, V., Egret, S., Doeuvre, L., Belliard, S., Eustache, F., Desgranges, B., Chetelat, G., 2013. Hippocampal subfield volumetry in mild cognitive impairment, Alzheimer's disease, and semantic dementia. Neuroimage Clin. 3, 155–162.

Lace, G., Savva, G.M., Forster, G., de Silva, R., Brayne, C., Matthews, F.E., Barclay, J.J., Dakin, L., Ince, P.G., Wharton, S.B., MRC-CFAS, 2009. Hippocampal tau pathology is related to neuroanatomical connections: an ageing population-based study. Brain 132, 1324–1334.

Li, S., Shi, F., Pu, F., Li, X., Jiang, T., Xie, S., Wang, Y., 2007. Hippocampal shape analysis of Alzheimer disease based on Machine LearningMethods. Am. J. Neuroradiol. 28, 1339–1345.

Li, X., Li, D., Li, Q., Li, Y., Li, K., Li, S., Han, Y., 2016. Hippocampal subfield volumetry in patients with subcortical vascular mild cognitive impairment. Sci. Rep. 6, 20873.

Mak, E., Su, L., Williams, G.B., Watson, R., Firbank, M., Blamire, A., O'Brien, J., 2016. Differential atrophy of hippocampal subfields: a comparative study of dementia with Lewy bodies and Alzheimer disease. Am. J. Geriatr. Psychiatry 24, 136–143.

Mckhann, G., Drachman, D., Folstein, M., Katzman, R., Price, D., Stadlan, E.M., 1984. Clinical-diagnosis of Alzheimers-disease - report of the NINCDS-ADRDA work group under the Auspices of Department-of-Health-and-human-Services Task-Force on Alzheimers-disease. Neurology 34, 939–944.

McKhann, G.M., Knopman, D.S., Chertkow, H., Hyman, B.T., Jack, C.R., Kawas, C.H., Klunk, W.E., Koroshetz, W.J., Manly, J.J., Mayeux, R., Mohs, R.C., Morris, J.C., Rossor, M.N., Scheltens, P., Carrillo, M.C., Thies, B., Weintraub, S., Phelps, C.H., 2011. The diagnosis of dementia due to Alzheimer's disease: recommendations from the National Institute on Aging-Alzheimer's Association workgroups on diagnostic guidelines for Alzheimer's disease. Alzheimers Dement. 7, 263–269.

Mesulam, M.M., Weintraub, S., Rogalski, E.J., Wieneke, C., Geula, C., Bigio, E.H., 2014. Asymmetry and heterogeneity of Alzheimer's and frontotemporal pathology in primary progressive aphasia. Brain 137, 1176–1192.

Mueller, S.G., Schuff, N., Yaffe, K., Madison, C., Miller, B., Weiner, M.W., 2010. Hippocampal atrophy patterns in mild cognitive impairment and Alzheimer's disease. Hum. Brain Mapp. 31, 1339–1347.

Mueller, S.G., Yushkevich, P.A., Das, S., Wang, L., Van Leemput, K., Iglesias, J.E., Alpert, K., Mezher, A., Ng, P., Paz, K., Weiner, M.W., 2018. Systematic comparison of different techniques to measure hippocampal subfield volumes in ADNI2. NeuroImage: Clin. 17, 1006–1018.

Musiek, E.S., Holtzman, D.M., 2015. Three dimensions of the amyloid hypothesis: time, space, and 'wingmen'. Nat. Neurosci. 18, 800–806.

Ossenkoppele, R., Jansen, W.J., Rabinovici, G.D., Knol, D.L., van der Flier, W.M., van Berckel, B.N.M., Scheltens, P., Visser, P.J., Grp, A.P.S., 2015. Prevalence of amyloid PET positivity in dementia syndromes: a meta-analysis. JAMA 313, 1939–1949.

Perneger, T.V., 1998. What's wrong with Bonferroni adjustments. BMJ 316, 1236–1238.

Perrotin, A., de Flores, R., Lamberton, F., Poisnel, G., La Joie, R., de la Sayette, V., Mezenge, F., Tomadesso, C., Landeau, B., Desgranges, B., Chetelat, G., 2015. Hippocampal subfield volumetry and 3D surface mapping in subjective cognitive decline. J. Alzheimers Dis. 48 (Suppl 1), S141–S150.

Price, J.L., Davis, P.B., Morris, J.C., White, D.L., 1991. The distribution of tangles, plaques and related immunohistochemical markers in healthy aging and Alzheimer's disease. Neurobiol. Aging 12, 295–312.

Raman, M.R., Preboske, G.M., Przybelski, S.A., Gunter, J.L., Senjem, M.L., Vemuri, P., Murphy, M.C., Murray, M.E., Boeve, B.F., Knopman, D.S., Petersen, R.C., Parisi, J.E., Dickson, D.W., Jack Jr., C.R., Kantarci, K., 2014. Antemortem MRI findings associated with microinfarcts at autopsy. Neurology 82, 1951–1958.

Rohrer, J.D., Rosen, H.J., 2013. Neuroimaging in frontotemporal dementia. Int. Rev. Psychiatry 25, 221–229.

Scheltens, P., Blennow, K., Breteler, M.M.B., de Strooper, B., Frisoni, G.B., Salloway, S., Van der Flier, W.M., 2016. Alzheimer's disease. Lancet 388, 505–517.

Scher, A.I., Xu, Y., Korf, E.S.C., White, L.R., Scheltens, 2007. Hippocampal shape analysis in Alzheimer's disease: a population-based study. Neuroimage 36, 8–18.

Schneider, J.A., Wilson, R.S., Bienias, J.L., Evans, D.A., Bennett, D.A., 2004. Cerebral infarctions and the likelihood of dementia from Alzheimer's disease pathology. Neurology 62, 1148–1156.

Schneider, J.A., Arvanitakis, Z., Bang, W., Bennett, D.A., 2007a. Mixed brain pathologies account for most dementia cases in community-dwelling older persons. Neurology 69, 2197–2204.

Schneider, J.A., Boyle, P.A., Arvanitakis, Z., Bienias, J.L., Bennett, D.A., 2007b. Subcortical infarcts, Alzheimer's disease pathology, and memory function in older persons. Ann. Neur. 62, 59–66.

Schneider, J.A., Arvanitakis, Z., Leurgans, S.E., Bennett, D.A., 2009. The neuropathology of probable Alzheimer disease and mild cognitive impairment. Ann. Neurol. 66, 200–208.

Schneider, J.A., Arvanitakis, Z., Yu, L., Boyle, P.A., Leurgans, S.E., Bennett, D.A., 2012. Cognitive impairment, decline, and fluctuations in older community-dwelling persons with Lewy bodies. Brain 135, 3005–3014.

Schönheit, B., Zarski, R., Ohn, T.G., 2004. Spatial and temporal relationships between plaques and tangles in Alzheimer-pathology. Neurobiol. Aging 25, 697–711.

Storandt, M., Mintun, M.A., Head, D., Morris, J.C., 2009. Cognitive decline and brain volume loss as signatures of cerebral amyloid-beta peptide deposition identified with Pittsburgh compound B: cognitive decline associated with Abeta deposition. Arch. Neurol. 66, 1476–1481.

Stoub, T.R., Bulgakova, M., Leurgans, S., Bennett, D.A., Fleischman, D., Turner, D.A., deToledo-Morrell, L., 2005. MRI Predictors of risk of incident Alzheimer disease: a longitudinal study. Neurology 64, 1520–1524.

Tepest, R., Wang, L., Csernansky, J.G., Neubert, P., Heun, R., Scheef, L., Jessen, F., 2008. Hippocampal surface analysis in subjective memory impairment, mild cognitive impairment, and Alzheimer's dementia. Dement Geriatr. Cogn. Disord. 26, 323–329.

Thaker, A.A., Weinberg, B., Dillon, W.P., Hess, C.P., Cabral, H.J., Fleischman, D.A., Leurgans, S.E., Bennett, D.A., Hyman, B.T., Albert, M.S., Killiany, R.J., Fischl, B., Dale, A.M., Desikan, R.S., 2017. Entorhinal cortex: ante-motrem cortical thickness and post-mortem neurofibrillary tangle and amyloid pathology. Am. J. Neuroradiol. 38, 961–965.

Tinetti, M.E., McAvay, G.J., Murphy, T.E., Gross, C.P., Lin, H., Allore, H.G., 2012. Contribution of individual diseases to death in older adults with multiple diseases. J. Am. Geriatr. Soc. 60, 1448–1456.

Toledo, J.B., Caims, N.J., Da, X., Chen, K., Carter, D., Fleisher, A., Householder, E., Ayutyanont, N., Roontiva, A., Bauer, R.J., Eisen, P., Shaw, L.M., Davatzikos, C., Weinger, M.W., Reiman, E.M., Morris, J.C., Trojanowski, J.Q., Alzheimer's Disease Neuroimaging Initiative (ADNI), 2013. Clinical and multimodal biomarker correlates of ADNI neuropathological findings. Acta Neuropathol. Commun. 1, 65.

Vemuri, P., Simon, G., Kantarci, K., Whitwell, J.L., Senjem, M.L., Pryzbelski, S.A., Gunter, J.L., Josephs, K.A., Knopman, D.S., Boeve, B.F., Ferman, T.J., Dickson, D.W., Parisi, J.E., Petersen, R.C., Jack Jr., C.R., 2011. Antemortem differential diagnosis of dementia pathology using structural MRI: Differential-STAND. Neuroimage 55, 522–531.

Villemagne, V.L., Fodero-Tavoletti, M.T., Masters, C.L., Rowe, C.C., 2015. Tau imaging: early progress and future directions. Lancet Neurol. 14, 114–124.

Wang, L., Swank, J.S., Glick, I.E., Gado, M.H., Miller, M.I., Morris, J.C., Csernansky, J.G., 2003. Changes in hippocampal volume and shape across time distinguish dementia of the Alzheimer type from healthy aging. Neuroimage 20, 667–682.

Wang, L., Miller, J.P., Gado, M.H., McKeel, D.W., Rothermich, M., Miller, M.I., Morris, J.C., Csernansky, J.G., 2006. Abnormalities of hippocampal surface structure in very mild dementia of the Alzheimer type. Neuroimage 30, 52–60.

Wang, L., Khan, A., Csernansky, J.G., Fischl, B., Miller, M.I., Morris, J.C., Beg, M.F., 2009. Fully-automated, multi-stage hippocampus mapping in very mild Alzheimer Disease. Hippocampus 19, 541–548.

Wang, L., Benzinger, T.L., Su, Y., Christensen, J., Friedrichsen, K., Aldea, P., McConathy, J., Cairns, N.J., Fagan, A.M., Morris, J.C., Ances, B.M., 2016. Evaluation of tau imaging in staging Alzheimer disease and revealing interactions between beta-amyloid and taupathy. JAMA Neurol. 73, 1070–1077.

Whitwell, J.L., Josephs, K.A., Murray, M.E., Kantarci, K., Pryzbelski, S.A., Weigand, S.D., Vemuri, P., Senjem, M.L., Parisi, J.E., KNopman, D.S., Boeve, B.F., Petersen, R.C., Dickson, D.W., Jack Jr., C.R., 2008. MRI correlates of neurofibrillary

tangle pathology at autopsy: a voxel-based morphometry study. Neurology 71, 743–749.
Wilson, A.C., Dugger, B.N., Dickson, D.W., Wang, D.S., 2011. TDP in aging and Alzheimer's disease – a review. Int. J. Clin. Exp. Pathol. 4, 147–155.
Wilson, R.S., Yu, L., Trojanowski, J.Q., Chen, E.Y., Boyle, P.A., Bennett, D.A., Schneider, J.A., 2013. TDP-43 pathology, cognitive decline, and dementia in old age. JAMA Neurol. 70, 1418–1424.
Worsley, K.J., 2005. An improved theoretical P value for SPMs based on discrete local maxima. Neuroimage 28, 1056–1062.
Worsley, K., Taylor, J., Carbonell, F., Chung, M., Duerden, E., Bernhardt, B., Boucher, M., Evans, A., 2009. SurfStat: A Matlab Toolbox for the Statistical Analysis of Univariate and Multivariate Surface and Volumetric Data Using Linear Mixed Effects Models and Random Field Theory. Paper Presented at: Organization for Human Brain Mapping. San Francisco, CA.
Yu, L., Boyle, P.A., Leurgans, S., Schneider, J.A., Bennett, D.A., 2014. Disentangling the effects of age and APOE on neuropathology and late life cognitive decline. Neurobiol. Aging 35, 819–826.
Yushkevich, P.A., Amaral, R.S., Augustinack, J.C., Bender, A.R., Bernstein, J.D., Boccardi, M., Bocchetta, M., Burggren, A.C., Carr, V.A., Chakravarty, M.M., Chetelat, G., Daugherty, A.M., Davachi, L., Ding, S.L., Ekstrom, A., Geerlings, M.I., Hassan, A., Huang, Y., Iglesias, J.E., La Joie, R., Kerchner, G.A., LaRocque, K.F., Libby, L.A., Malykhin, N., Mueller, S.G., Olsen, R.K., Palombo, D.J., Parekh, M.B., Pluta, J.B., Preston, A.R., Pruessner, J.C., Ranganath, C., Raz, N., Schlichting, M.L., Schoemaker, D., Singh, S., Stark, C.E., Suthana, N., Tompary, A., Turowski, M.M., Van Leemput, K., Wagner, A.D., Wang, L., Winterburn, J.L., Wisse, L.E., Yassa, M.A., Zeineh, M.M., for the Hippocampal Subfields, G., 2015. Quantitative comparison of 21 protocols for labeling hippocampal subfields and parahippocampal subregions in in vivo MRI: towards a harmonized segmentation protocol. Neuroimage 111, 526–541.
Zarow, C., Wang, L., Chui, H.C., Weiner, M.W., Csernansky, J.G., 2011. MRI shows more severe hippocampal atrophy and shape deformation in hippocampal sclerosis than in Alzheimer's disease. Int. J. Alzheimers Dis. 2011, 483972.